Structural Basis for the Binding of the Anticancer Compound 6-(7-Nitro-2,1,3-Benzoxadiazol-4-Ylthio)Hexanol to Human Glutathione *S*-Transferases

Luca Federici,[1] Carlo Lo Sterzo,[2] Silvia Pezzola,[3] Adele Di Matteo,[2] Flavio Scaloni,[2] Giorgio Federici,[4] and Anna Maria Caccuri[3]

[1]Ce.S.I. Center of Excellence on Aging, "G. D'Annunzio" University Foundation and Department of Biomedical Sciences, University of Chieti, Chieti, Italy; [2]Department of Biochemical Sciences, "Sapienza" University of Rome; [3]Department of Chemical Sciences and Technologies and [4]Departments of Internal Medicine and Laboratory Medicine, Policlinico di Tor Vergata, University of Rome "Tor Vergata", Rome, Italy

Abstract

Glutathione *S*-transferases (GST) constitute a superfamily of enzymes with diversified functions including detoxification from xenobiotics. In many human cancers, Pi class GST (GSTP1-1) is overexpressed and contributes to multidrug resistance by conjugating chemotherapeutics. In addition, GSTP1-1 displays antiapoptotic activity by interacting with c-*Jun* NH_2-terminal kinase, a key regulator of apoptosis. Therefore, GSTP1-1 is considered a promising target for pharmaceutical treatment. Recently, a potent inhibitor of GSTs, 6-(7-nitro-2,1,3-benzoxadiazol-4-ylthio)hexanol (NBDHEX), was identified and tested on several tumor cell lines demonstrating high antiproliferative activity. To establish the structural basis of NBDHEX activity, we determined the crystal structure of NBDHEX bound to either GSTP1-1 or GSTM2-2 (mu class). NBDHEX in both cases binds to the H-site but occupies different positions. Furthermore, the compound is covalently attached to the GSH sulfur in the GSTM2-2 crystal, forming a σ-complex, although it is bound but not conjugated in the GSTP1-1 crystal. Several differences in the H-sites of the two isozymes determine the higher affinity of NBDHEX for GSTM2-2 with respect to GSTP1-1. One such difference is the presence of Ile^{104} in GSTP1-1 close to the bound NBDHEX, whereas the corresponding position is occupied by an alanine in GSTM2-2. Mutation of Ile^{104} into valine is a frequent GSTP1-1 polymorphism and we show here that the Ile^{104}Val and Ile^{104}Ala variants display a 4-fold higher affinity for the compound. Remarkably, the GSTP1-1/Ile^{104}Ala structure in complex with NBDHEX shows a considerable shift of the compound inside the H-site. These data might be useful for the development of new anticancer compounds. [Cancer Res 2009;69(20):8025–34]

Introduction

Multidrug resistance in cancer treatment is commonly defined as the capacity of a cancer cell to develop simultaneous resistance to several chemotherapeutic agents. One common mechanism through which cancer cells may achieve multidrug resistance is the overexpression of glutathione *S*-transferases (GST; refs. 1, 2).

Requests for reprints: Luca Federici, Ce.S.I. Center of Excellence on Aging, University of Chieti "G. D'Annunzio", Via Colle dell'Ara, 66100 Chieti, Italy. Phone: 39-87154-1414; Fax: 39-87154-1598; E-mail: lfederici@unich.it.

doi:10.1158/0008-5472.CAN-09-1314

GSTs constitute a superfamily of enzymes with diversified functions (3, 4). These enzymes are known to decrease the pharmacologic activity of a wide range of structurally unrelated drugs through their conjugation with glutathione (GSH). Furthermore, the GS-conjugated compounds may be actively extruded from the cell through specialized pumps; principally, the multidrug resistance proteins MRP-1 and MRP-2 (ABCC1, ABCC2; ref. 1).

In humans, several GST isoforms are differentially expressed and are subdivided into different classes (5). The Pi class GSTP1-1 is overexpressed in a variety of different human malignancies including lung (6), colon (7), stomach (8), kidney (9), ovary (10), mouth (11), and testis (12) cancers. Furthermore, in some cases, GSTP1-1 overexpression has been linked to acquired multidrug resistance to chemotherapeutic agents including cisplatin, adriamycin, etoposide, thiotepa, chlorambucil, and ethacrynic acid (1, 13). This phenotype may arise from the conjugating activity of the enzyme but also because GSTP1-1 displays a "nonenzymatic" antiapoptotic activity through its interaction with the c-*Jun* NH_2-terminal kinase (JNK), a key enzyme in the apoptotic cascade (14, 15). Because GSTP1-1 binds JNK through its COOH-terminal region, which contributes to shaping the hydrophobic substrate binding site (H-site), inhibitors that target this site, together with inactivating the enzyme, might also dissociate its complex with JNK and activate the JNK apoptotic pathway (16, 17). Therefore, GSTP1-1 is considered as a promising target for inactivation in cancer treatment and numerous groups have spent considerable effort finding potent inhibitors of this enzyme (18, 19).

Recently, a new class of nonpeptidomimetic inhibitors of human GSTs has been identified based on 7-nitro-2,1,3-benzoxadiazole ring derivatives (20). Among these, the compound 6-(7-nitro-2,1,3-benzoxadiazol-4-ylthio)hexanol (NBDHEX) has been shown to inhibit GST isoforms at micromolar or submicromolar amounts and to induce apoptosis in several tumor cell lines by dissociating the GSTP1-1/JNK complex (20, 21). Moreover NBDHEX is able to overcome the P-glycoprotein and MRP1 associated resistance in leukemia (22, 23) and small cell lung cancers (24) and also to overcome the GSTP1-1–related cisplatin resistance in osteosarcoma (25), suggesting that it might be used to treat a number of cancers in combination with other drugs.

A detailed functional analysis of the mode of action of NBDHEX indicated that this compound behaves like a suicide substrate of GSTs through the formation of a σ-complex with GST-bound GSH. In this complex, the GSH sulfur is thought to conjugate the NBDHEX benzoxadiazole ring at its C4, which assumes a tetrahedral conformation by retaining the hexanol

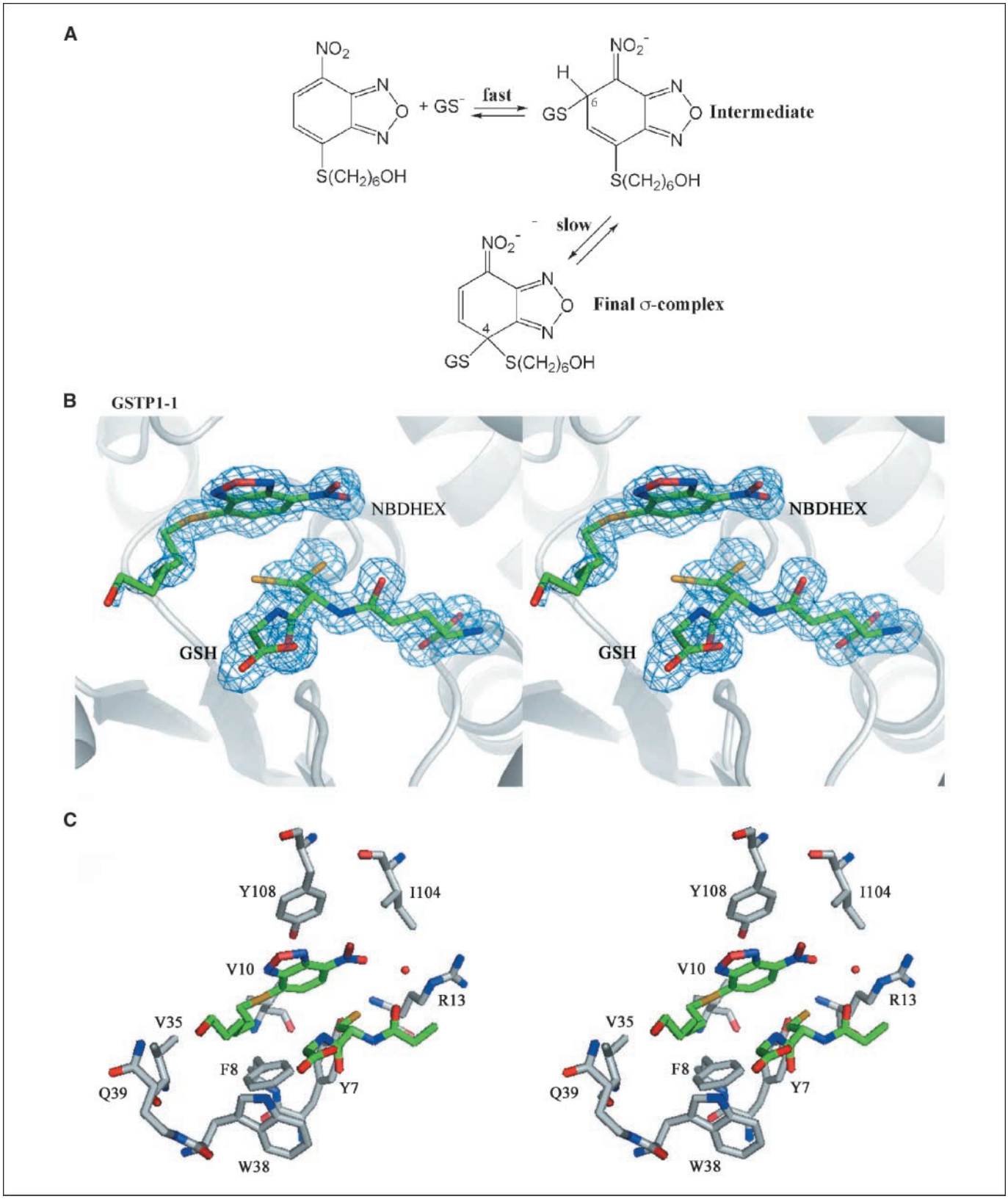

Figure 1. *A,* proposed mechanism of σ-complex formation between NBDHEX and the GST-bound GSH on the basis of kinetics data (20). *B,* crystal structure of the GSTP1-1/GSH/NBDHEX complex. Stereoview of the GSTP1-1 active site (chain A). GSH and NBDHEX (*sticks*); the σ_A-weighted 2Fo-Fc map, contoured at 1.0 σ (*blue mesh*). No continuous electron density was observed between the NBDHEX molecule and the GSH sulfur atom. Furthermore, electron density accounts for a double conformation of the GSH sulfur atom. *C,* detailed view of the active site architecture. NBDHEX and GSH (*sticks with green carbons*). The GSH sulfur atom is represented only in its main conformation (75% of occupancy) for clarity. Residues in the proximity of NBDHEX (*sticks with white carbons*). The water molecule bridging Arg[13] with the benzoxadiazole nitro group (*red sphere*).

moiety (Fig. 1*A*; ref. 20). This intermediate is stable into the GSTP1-1, but also into the mu class GSTM2-2 active sites and thus inactivates both enzymes (20).

One of the issues raised by the use of GST inhibitors is their specificity (18). In principle, because the major role in cancer is played by GSTP1-1, a specific inhibitor for this particular isozyme would be desirable. Unfortunately, NBDHEX seems to be less specific for GSTP1-1 (IC_{50} = 0.80 μmol/L) than for GSTM2-2 (IC_{50} < 0.01 μmol/L; 20). In this work, we investigated how NBDHEX binds to both GSTP1-1 and GSTM2-2, and we present the crystal structures of the GSTP1-1/GSH/NBDHEX and GSTM2-2/GSH/NBDHEX complexes.

NBDHEX binds tightly to the enzymes' H-sites, but occupies different positions due to the molecular architecture of the H-site in the two isozymes. Furthermore, whereas a σ-complex was observed in the GSTM2-2 isozyme, a preconjugation state was observed with GSTP1-1. Finally, we investigated the role played in GSTP1-1 by the common $Ile^{104}Val$ polymorphism (26) and by the $Ile^{104}Ala$ mutation, that mimics the residue occupying this position in GSTM2-2. We determined the structure of the GSTP1-1/$Ile^{104}Ala$ variant in complex with NBDHEX and we show that this mutation is sufficient to cause a considerable shift of the NBDHEX position within the H-site. Our data provides a rational basis for explaining the differential affinity of NBDHEX towards GST isoforms and paves the way for the rational design of new derivatives with increased affinity and specificity for GSTP1-1.

Materials and Methods

Site-directed mutagenesis, expression, and purification. The GSTP1-1/Val^{104} and GSTP1-1/Ala^{104} variants were obtained using the QuickChange kit (Stratagene) and plasmid pGST1 (27). The following forward primers were used:

I104V Fw 5′-CCTCCGCTGCAAATACGTCTCCCTCATCTACAC-3′
I104A Fw 5′-GACCTCCGCTGCAAATACGCCTCCCTCATCTACACCAAC-3′

Human GSTM2-2, GSTP1-1/Ile^{104}, GSTP1-1/Val^{104}, and GSTP1-1/Ala^{104} were expressed in *Escherichia coli* and purified as previously described (28).

Crystallization. GSTP1-1 and GSTM2-2 were concentrated to 10 mg/mL in 10 mmol/L of Hepes (pH 7.0). Experiments were performed after pretreating the protein solution with 5 mmol/L of GSH (Sigma), alone or in combination with NBDHEX (100–500 μmol/L). NBDHEX was synthesized as previously described (20).

GSTM2-2/GSH/NBDHEX cocrystals were obtained by vapor diffusion using the following mother liquor: PEG8000 16% w/v, 100 mmol/L of MES (pH 6.0), and 200 mmol/L of NaCl. Crystals were cryoprotected by transfer into a mother liquor containing the appropriate amounts of GSH and NBDHEX plus 20% ethylene glycol.

GSTP1-1/GSH/NBDHEX cocrystals, grown using PEG8000 as a precipitating agent, were of poor quality and did not diffract satisfactorily. Therefore, GSTP1-1/GSH crystals were grown and then soaked with NBDHEX. GSTP1-1/GSH cocrystals were grown at 4.0°C using 1.8 mol/L of ammonium sulfate as a precipitating agent in 100 mmol/L of MES buffer (pH 6.0). Crystals were then soaked with NBDHEX (100–500 μmol/L). A mother liquor solution containing the appropriate amounts of GSH and NBDHEX plus 20% glycerol was used for cryoprotection. GSTP1-1/Ala^{104} crystals were grown, soaked, and cryoprotected using the same protocols as the wild-type protein.

Data collection and processing. GSTM2-2 complete data were collected to 2.5 Å resolution at the BL14-1 beamline of the BeSSY Synchrotron (Berlin, Germany). The crystals belong to the orthorhombic space group $P2_12_12_1$ and contain two GSTM2-2 dimers in the asymmetric unit.

GSTP1-1 data were collected to 1.55 Å resolution at the ID14-1 beamline of the European Synchrotron Research Facility (ESRF, Grenoble, France). Crystal belongs to the space group C2 and contains one GSTP1-1 dimer in the asymmetric unit. GSTP1-1/Ala^{104} data were collected to 1.8 Å resolution at the ID14-2 beamline of the ESRF Synchrotron. Crystals were isomorphous to wild-type protein crystals. Data were processed with Denzo and scaled with Scalepack (29). Statistics about data collection and processing are reported in Table 1.

Structure determination and refinement. The GSTM2-2/GSH/NBDHEX complex structure was determined by molecular replacement using the program MOLREP (30) and the GSTM2-2 dimer (in the absence of GSH; pdb code:1HNC; ref. 31) as a search model. After initial refinement using the program REFMAC (32), electron density maps were examined using the program COOT (33). Positive electron density in the Fo-Fc map was found in all four subunits, accounting for the presence of GSH. Additional positive electron density was found in the H-site of subunits A and C. This electron density was continuous between the GSH sulfur and the H-site suggesting the presence of a σ-complex between NBDHEX and GSH, which was modeled in chain C with full occupancy and in chain A with half occupancy. The model was refined to 2.5 Å resolution by several stages of restrained refinement in REFMAC, maps inspection, and model adjustments. The final model has an R_{factor} of 21.3% and an R_{free} of 27.3%.

The GSTP1-1/GSH/NBDHEX–soaked crystal was isomorphous with the native GSTP1-1 crystal (pdb code: 6GSS; ref. 34). Therefore, the native GSTP1-1 dimer was used for refinement using REFMAC in the absence of any ligand. Inspection of the Fo-Fc positive difference map indicated the presence of GSH and NBDHEX in both subunits, which were not covalently bound. The structure was refined to 1.55 Å resolution iteratively by using REFMAC and COOT. The final model is refined with an R_{factor} of 16.9% and an R_{free} of 19.5%. The GSTP1-1/Ala^{104} structure in complex with NBDHEX and GSH was obtained using the same procedure as the wild-type protein and refined to a final R_{factor} of 17.9% and an R_{free} of 20.9%.

The quality of all models was assessed using COOT and Procheck (35). Table 1 reports statistics on refinement and model quality. Model coordinates and structure factors have been deposited in the PDB with accession codes: 3GUR (for the GSTM2-2 structure), 3GUS (for GSTP1-1), and 3IE3 (for GSTP1-1/Ala^{104}).

Binding of NBDHEX to GSTs. GST activity was assayed at 25°C as previously reported (36). The affinities of NBDHEX for GSTP1-1/Ile^{104} (wild-type), GSTP1-1/Val^{104}, and GSTP1-1/Ala^{104} were determined in the presence of 1 mmol/L of GSH. The quenching of the intrinsic fluorescence of the protein (excitation at 295 nm and emission at 340 nm) was measured in a single photon counting spectrofluorometer (Perkin-Elmer LS50B) at 25°C after the addition of variable amounts of NBDHEX to 4 μmol/L GST in 0.1 mol/L of potassium phosphate buffer (pH 6.5), containing 1 mmol/L of GSH. Fluorescence data were corrected for inner filter effects and fitted to Eq. A, which yields the apparent dissociation constant (K_D) for the NBDHEX bound to GST,

$$\Delta F = \Delta F_{max}/(1 + K_D/[\mathrm{NBDHEX}]^{nH}) \qquad (A)$$

where ΔF is the protein fluorescence change observed in the presence of a given amount of NBDHEX, ΔF_{max} is the maximum fluorescence change observed at saturating NBDHEX concentration, and *nH* is the Hill coefficient.

Spectrophotometric analysis. The interaction of NBDHEX with GSTs and GSH was analyzed as previously reported (20). The UV-visible spectrum of NBDHEX (50 μmol/L) in 0.1 mol/L of potassium phosphate buffer (pH 6.5), containing 1 mmol/L of GSH was recorded at 25°C before and after the addition of GSTP1-1/Ile^{104}, GSTP1-1/Val^{104}, or GSTP1-1/Ala^{104} (100 μmol/L).

Results

Structure of the GSTP1-1/GSH/NBDHEX complex. We obtained the crystal structure of the GSTP1-1/GSH/NBDHEX

Table 1. Data collection and refinement statistics

	GSTM2-2	GSTP1-1	GSTP1-1/Ala^{104}
Data collection			
Beamline	BeSSY BL14-1	ESRF ID14-1	ESRF ID14-2
Wavelength (Å)	0.9184	0.9340	0.9330
Resolution (Å)*	29.43–2.5 (2.59–2.5)	30.0–1.55 (1.61–1.55)	29.21–1.80 (1.86–1.80)
Space group	$P2_12_12_1$	C2	C2
Unit cell dimensions (Å)	a = 56.75	a = 78.59	a = 77.87
	b = 78.02	b = 89.35	b = 89.53
	c = 219.36	c = 69.26	c = 68.92
		β = 98.36 degrees	β = 98.04 degrees
Unique reflections	32,108	67,852	42,435
Redundancy	4.8	2.6	4.0
Completeness (%)*	93.2 (83.1)	96.8 (96.5)	99.1 (99.0)
Average (I/σ)*	18.32 (7.01)	9.47 (5.06)	17.38 (8.05)
R_{merge} (%)*, †	8.6 (10.0)	5.3 (26.0)	5.8 (17.8)
Refinement			
Resolution range (Å)	29.43–2.5	30.0–1.55	29.21–1.80
R_{cryst} (%)	21.3	16.9	17.9
R_{free} (%) ‡	27.3	19.5	20.9
Mean B factors (Å)^2			
Protein main chain	26.0	12.1	13.0
Protein side chain	26.4	13.5	14.0
Waters	20.6	26.7	22.5
GSH	25.1 (chains B and D)	13.3	13.4
NBDHEX		34.6	32.8
NBDHEX-GS σ-complex	34.1 (chains A and C)		
Rms deviation length (Å)	0.009	0.008	0.007
Rms deviation angle (degrees)	1.45	1.49	1.37
Ramachandran statistics			
Residues in favored regions (%)	91.5	93.3	93.0
Residues in allowed regions (%)	8.5	6.7	7.0
Residues in disallowed regions (%)	0.0	0.0	0.0

*Numbers in parentheses refer to the last resolution shell.
† $R_{merge} = \Sigma_{hkl}\Sigma_i|I_i - \langle I\rangle|/|\langle I\rangle|$, with I_i being the intensity for the ith measurement of an equivalent reflection with indices h,k,l.
‡ R_{free} was calculated on 5% of data excluded before refinement.

complex at 1.55 Å resolution from a crystal that was grown in the presence of protein and GSH only, and subsequently soaked with NBDHEX, because cocrystallization experiments with both NBDHEX and GSH did not lead to well-diffracting crystals. Figure 1*B* shows NBDHEX bound to the protein H-site in proximity to the bound GSH. The crystal asymmetric unit contains a physiologic GSTP1-1 dimer and clear density for NBDHEX was observed in both monomers. The NBDHEX molecule was clearly visible in the electron density, including most of the 6-mercapto-hexanol moiety atoms (Fig. 1*B*). The two NBDHEX benzoxadiazole rings occupy the same position in the H-sites of both chains with rms deviations between equivalent atoms of <0.15 Å, whereas the hexanol moiety atoms have a rms deviation of 0.62 Å.

NBDHEX is oriented in the H-site with the nitro group placed deep inside the interior of the protein and the hexanol moiety facing the active site opening to the solvent (Fig. 1*B*). Several hydrophobic interactions were found involving residues shaping the H-site including Tyr^7, Phe^8, Val^{35}, Trp^{38}, Gln^{39}, Ile^{104}, and above all, Tyr^{108}, which engages an aromatic ring stacking interaction with the NBDHEX benzoxadiazole ring (Table 2; Fig. 1*C*). The main contribution to the molecule stabilization and orientation in the H-site is likely provided by interaction of the benzoxadiazole ring NO_2 group with Arg^{13}. This interaction was not direct but was mediated by a water molecule (*red sphere,* Fig. 1*C*). This water molecule is found in exactly the same position in both monomers and its structural role is confirmed by an average B-factor of 13.05 Å^2, a value in the range of main chain protein atoms' B-factors. The water molecule is hydrogen-bonded both to Arg^{13} Nε, being at a distance of 2.9 Å, and to the benzoxadiazole NO_2 group, being at a distance of 2,6 Å from the closest oxygen.

In our maps, we did not find any trace of continuous electron density connecting the GSH sulfur and NBDHEX. This finding prompted us to exclude the presence of a GSH/NBDHEX σ-complex in this crystal (Fig. 1*B*). Therefore, in our structure, we observe a bound but not conjugated NBDHEX. This was quite surprising because the formation of a GSH/NBDHEX σ-complex in the GSTP1-1 active site can be easily monitored in solution by absorption spectra (20). However, it was previously suggested by kinetic studies that, in the reaction between GSH and either CDNB (37) or 7-chloro-4-nitrobenzo-2-oxa-1,3-diazole (NBD-Cl; ref. 38), a physical event, i.e., a conformational change in GSTP1-1 structure, follows the binding of the substrates and is crucial for the

σ-complex formation. This conformational transition is strongly dependent on diffusion-controlled motion of active site regions. Because NBDHEX retains the same benzoxadiazole ring as NBD-Cl, a similar conformational change might also be necessary in this case to enable the σ-complex formation, and this might be prevented by a lack of structural flexibility in the crystalline environment.

Nonetheless, the position of NBDHEX with respect to GSH is very interesting. In fact, it has been hypothesized, on the basis of kinetics data, that the formation of the σ-complex, in which the GSH sulfur is bound to the benzoxadiazole C4 (the same carbon that binds the 6-mercapto-hexanol moiety sulfur) is the rate-limiting step of a reaction that first involves the nucleophilic addition of the GSH sulfur to the C6 atom of the benzoxadiazole ring; this covalent complex then evolves to the more stable σ-complex (Fig. 1*A*; ref. 20). Indeed, in our structure, we observe that the GSH sulfur adopts two distinct conformations (Fig. 1*B*). In the main one, which accounts for 75% of total occupancy, the GSH sulfur is at 3.1 Å distance from the NBDHEX C6, whereas it is at 4.9 Å distance from the C4. In the second conformation, which accounts for the remaining 25% of occupancy, the GSH sulfur is closer to the NBDHEX C4 (3.1 Å). Therefore, we can conclude that (*a*) our electron density maps seem to be consistent with the hypothesized mechanism and depict the position of a preconjugation state and (*b*) the formation of the stable σ-complex may be described without invoking major movements of the NBDHEX benzoxadiazole ring from its current position. In fact, a simple rotation of the GSH sulfur is consistent with its nucleophilic attack to the benzoxadiazole C4.

Structure of the GSTM2-2/GSH/NBDHEX complex. The structure of the GSTM2-2/GSH/NBDHEX complex was determined at 2.50 Å resolution. In this case, additional electron density accountable for the presence of the compound was visible only in one monomer for each asymmetric unit dimer (chains A and C). As expected, NBDHEX binds to the H-site. Electron density maps clearly indicate the position of the benzoxadiazole ring, whereas the hexanol moiety is only partially visible (Fig. 2*A*). The two NBDHEX benzoxadiazole rings modeled in chains A and C occupy exactly the same position with rms deviations among equivalent atoms <0.20 Å. NBDHEX is oriented in the same way as in the complex with GSTP1-1, with the benzoxadiazole NO_2 facing the interior of the protein and the hexanol moiety facing the H-site opening. A stacking interaction between the benzoxadiazole ring and Tyr^{115} strongly contributes to the NBDHEX orientation and stabilization (Fig. 2*B*). Several other hydrophobic interactions involve residues shaping the H-site, including Tyr^{6}, Trp^{7}, Gly^{11}, and Leu^{12} (Table 2). As in the GSTP1-1 cocrystal, the main contribution to NBDHEX stabilization is provided by interactions involving the benzoxadiazole NO_2 group. In this structure in fact, the NO_2 group is at close distance from two arginines, Arg^{107} and Arg^{165} (Fig. 2*B*). In particular, the Arg^{165} NH1 atom is at 3.0 Å distance from the closest NO_2 oxygen, establishing a direct H-bond interaction, whereas the same NO_2 oxygen atom is at 3.4 Å distance from the Arg^{107} NH1 atom. Therefore, both residues cooperate to stabilize the NO_2 group that is negatively charged when the σ-complex is formed.

Importantly, in this crystal, we could see continuous electron density spanning from the GSH sulfur to the C4 carbon of the benzoxadiazole ring (Fig. 2*A*), indicating the presence of a σ-complex and thus providing an independent experimental clue to the proposed mechanism of inhibition (20).

Comparison between the two complexes. The electrostatic potential surfaces of GSTP1-1 and GSTM2-2 are shown in Fig. 3*A* and *B*, respectively. The NBDHEX molecule perfectly adapts to the GSTP1-1 H-site profile, with its benzoxadiazole ring being parallel to the active site "ceiling" that is made by Tyr^{108}. The hexanol moiety also follows the active site shape because of its hydrophobic interactions with Phe^{8} and Trp^{38} and of a weak hydrogen bond (3.3 Å distance) between Gln^{39} and the hexanol oxydryl group (Fig. 1*C*). The H-site in the GSTM2-2 structure appears differently shaped from that of GSTP1-1, with a deeper cavity toward the core of the protein, which is occupied by the NBDHEX nitro group (Fig. 3*B*). This different H-site shape mainly results from the presence of residues Ile^{104} and Arg^{13} in the GSTP1-1 H-site, that face the NBDHEX nitro group in the complex (Fig. 1*C*). GSTP1-1 Ile^{104} and Arg^{13} are topologically replaced by an alanine (Ala^{111}) and a

Table 2. Residues within 4.5 Å from NBDHEX

Residue	Distance*	Interaction type
GSTM-2		
Tyr^{6}	2.5	Arom
Trp^{7}	4.3	Arom
Ile^{9}	4.4	Phob
Gly^{11}	3.4	—
Leu^{12}	3.5	H-Phob
Met^{34}	3.9	Phob
Arg^{42}	4.5	H-Phob
Arg^{107}	3.4	HB
Ala^{111}	3.6	H-Phob
Tyr^{115}	3.6	Arom
Arg^{165}	3.0	HB
Phe^{208}	3.4	Arom
Thr^{209}	3.1	Phob
Met^{211}	4.4	Phob
GSTP1-1		
Tyr^{7}	3.9	Arom
Phe^{8}	3.6	Arom
Arg^{13}	4.4	HB (water-mediated)
Val^{35}	4.0	Phob
Trp^{38}	3.6	Phob
Gln^{39}	3.3	HB
Ile^{104}	3.4	H-Phob
Tyr^{108}	3.3	Arom
GSTP1-1/Ala^{104}		
Tyr^{7}	4.1	Arom
Phe^{8}	3.7	Phob
Arg^{13}	2.9	HB (direct)
Val^{35}	4.4	Phob
Trp^{38}	4.3	Phob
Gln^{39}	3.7	HB
Ala^{104}	3.5	—
Tyr^{108}	3.2	Arom
Gly^{205}	3.9	H-Phob

NOTE: Interaction types: HB, hydrophilic-hydrophilic (H-bond); Arom, aromatic-aromatic; Phob, hydrophobic-hydrophobic; H-Phob, hydrophilic-hydrophobic.

*Distances are the average of those relative to the different monomers in the same structure and were calculated using the program LPC/CSU (http://ligin.weizmann.ac.il/cgi-bin/lpccsu/LpcCsu.cgi).

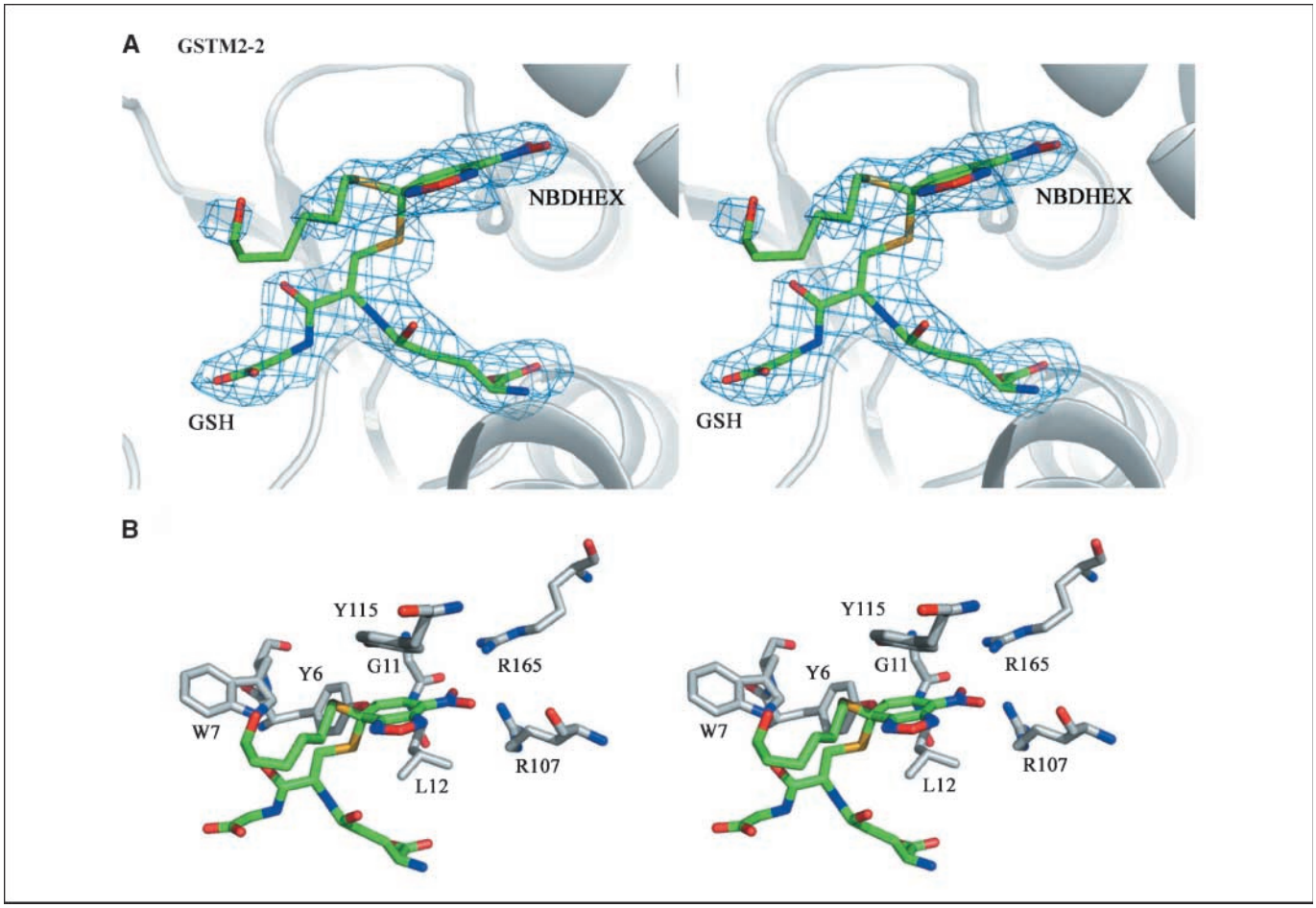

Figure 2. Crystal structure of the GSTM2-2/GSH/NBDHEX complex. *A,* stereoview of the GSTM2-2 active site (chain C). The σ_A-weighted 2Fo-Fc map, contoured at 1.0 σ (*blue mesh*); GSH and NBDHEX (*sticks*). A σ-complex is observed in this case in the electron density map, with the GSH sulfur atom covalently bound to the benzoxadiazole ring C4, which assumes a tetrahedral conformation. *B,* detailed view of the active site architecture. The GSH/NBDHEX σ-complex (*sticks with green carbons*). Residues facing the active site (*sticks with white carbons*). Two positively charged residues (*R107* and *R165*) are at binding distance from the negatively charged nitro group of NBDHEX.

leucine (Leu^{12}), respectively, in the GSTM2-2 structure (Fig. 3*C*), and the presence here of these less cumbersome residues allows the NBDHEX molecule to move further and for its nitro group to interact directly with the positively charged Arg^{107} and Arg^{165} (Figs. 2*B* and 3*C*). Arg^{107} is conserved in GSTP1-1 (Arg^{100}) but its access to the H-site is hindered by Ile^{104}, whereas the GSTM2-2 Arg^{165} is topologically replaced by an isoleucine (Ile^{161}) in GSTP1-1 (Fig. 3*C*).

The superposition between the two structures also highlights that the NBDHEX molecules do not occupy the same position in the two H-sites (Fig. 3*C*). The rms deviation among equivalent atoms of the two NBDHEX benzoxadiazole rings is 4.25 Å in the superimposed structures, and a major shift plus a rotation are required to superpose the free NBDHEX of GSTP1-1 to the one covalently bound to GSH in the GSTM2-2 σ-complex (Fig. 3*C*). This movement, however, is unrealistic because the hydrophobic side chain of Ile^{104} is only 3.4 Å apart from the benzoxadiazole nitro group in the GSTP1-1 complex and provides steric hindrance (Figs. 1*B* and 3*C*). Taken together, our data suggests that the GSH/NBDHEX σ-complex in the GSTP1-1 structure would occupy a different position from the one experimentally observed in the GSTM2-2 cocrystal. This is confirmed by the observation that a simple rotation of the GSH cysteine side chain in GSTP1-1 is sufficient to place the sulfur atom in a position competent for addition to the benzoxadiazole C4 (Fig. 1*B*).

A $Ile^{104}Val$ allelic variation of GSTP1-1 increases the isozyme's affinity for NBDHEX. Residue Ile^{104} of GSTP1-1 faces the benzoxadiazole nitro group and constitutes a physical obstacle to its movement towards the positive charges at the H-site bottom (Figs. 1*C* and 3*C*). This finding immediately captured our attention because mutation of Ile^{104} into valine is a common polymorphism of human GSTP1-1 and is frequent in tumors (26). To better assess the role of Ile^{104} with respect to NBDHEX binding and activity, we mutated it into valine (GSTP1-1/Val) and alanine, which is the residue present at this position in GSTM2-2 (GSTP1-1/Ala; Fig. 3*C*).

The specific activities for CDNB of the GSTP1-1/Val and GSTP1-1/Ala mutant enzymes were 58 $\pm$ 2 and 47 $\pm$ 3 μmol/min/mg, respectively. These values are approximately twice lower than those obtained with wild-type GSTP1-1/Ile^{104} (100 $\pm$ 2 μmol/min/mg; ref. 39). Binding of NBDHEX, in the presence of 1 mmol/L of GSH, followed a hyperbolic behavior (Hill coefficient *nH* 1.0) with GSTP1-1/Ala^{104} and a slight cooperative trend (Hill coefficient *nH* 0.8) with GSTP1-1/Val^{104}.

Remarkably, NBDHEX bound to GSTP1-1/Val^{104} with a dissociation constant of 0.26 $\pm$ 0.07 μmol/L, a value comparable to that of

GSTP1-1/Ala^{104} (0.21 ± 0.06 μmol/L) and approximately four times lower than that of GSTP1-1/Ile^{104} (K_D = 0.90 ± 0.08 μmol/L; ref. 20; Fig. 4*A*). This indicates that replacement of Ile^{104} with a less bulky residue increases the affinity of the enzyme towards NBDHEX.

As previously shown with GSTP1-1/Ile^{104} (20), a remarkable change in the NBDHEX spectrum was observed in the presence of both Val and Ala GSTP1-1 variants. When NBDHEX was incubated with two equivalents of GSTP1-1/Val^{104} or GSTP1-1/Ala^{104} in the presence of 1 mmol/L of GSH, the UV-visible spectrum of NBDHEX, centered at 432 nm, completely disappeared and a new absorption band appeared between 340 and 350 nm (Fig. 4*B*). No spectral changes were observed in the absence of GSH. The extinction coefficient was approximately the same for the Ala^{104}, Val^{104}, and Ile^{104} GSTP1-1 variants, suggesting that NBDHEX forms a stable σ-complex with GSH in all cases. Interestingly, a blue-shift of ~6 nm was observed for the maximum absorption in the GSTP1-1/Ala^{104} spectrum (Fig. 4*B*). This led us to hypothesize that the compound might be slightly shifted in this mutant isozyme with respect to the other two natural variants. To test this hypothesis, we determined the structure of the GSTP1-Ala^{104}/GSH/NBDHEX complex to a resolution of 1.8 Å (Fig. 4*C*). As for the wild-type, we observe a Michaelis complex with the compound bound but not conjugated and a single conformation is found for the GSH sulfur that corresponds to the main conformation observed in the wild-type crystal. The main aspect of this structure is that, as hypothesized, NBDHEX is shifted towards the interior of the site and its nitro group is at hydrogen bond distance (2.9 Å) from the Arg^{13} Nε, whereas the water molecule that bridged the NBDHEX nitro group and Arg^{13} in the wild-type structure, is displaced. A superposition of the GSTP1-1/Ile^{104} and GSTP1-1/Ala^{104} structures (Fig. 4*D*) highlights the different position occupied by the two NBDHEX-bound molecules with an average distance of 1.87 Å between the same atoms of the two benzoxadiazole rings, whereas the rms deviation among Cα in the two superimposed structures is only 0.14 Å.

Discussion

In this work, we tackled the problem of specificity in GST inhibition and focused our attention on NBDHEX, a compound that is currently being investigated for the treatment of several cancers (21–25). Our major goal was to understand the structural basis of the different affinities of NBDHEX for human GST isozymes and gain the knowledge to rationally design molecules that are specific for GSTP1-1. For this purpose, we determined the crystal structure of NBDHEX in complex with GSTP1-1 but also

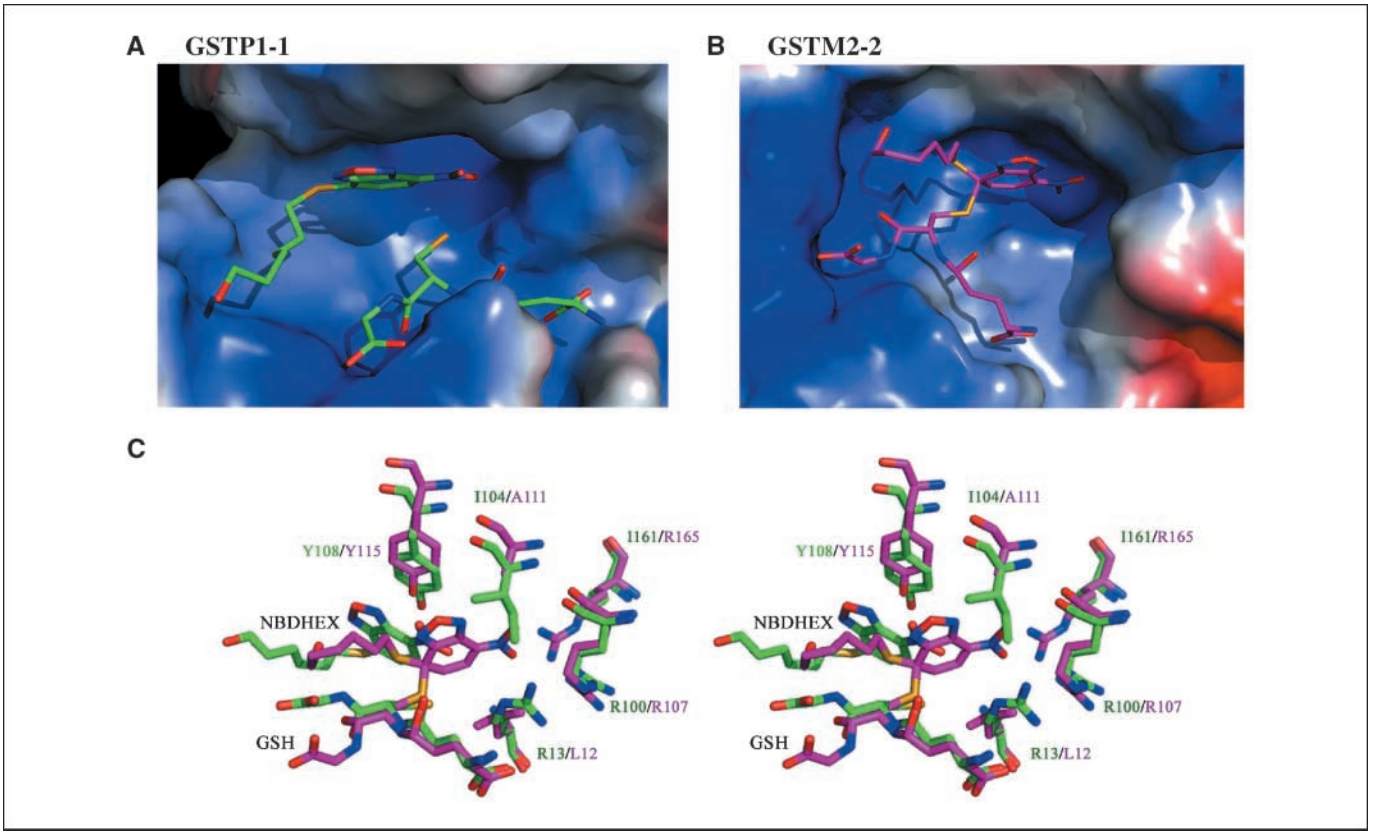

Figure 3. Comparison between the GSTP1-1 and GSTM2-2 active sites. *A,* electrostatic potential surface representation of the GSTP1-1 active site. Positive charge distribution (*blue*), negative charge (*red*), and hydrophobic surface (*white*). NBDHEX and GSH (*sticks with green carbons*). NBDHEX adapts to the shape of the GSTP1-1 H-site ceiling with the benzoxadiazole ring nitro group facing a hydrophobic surface area contributed by GSTP1-1 Ile^{104}. *B,* electrostatic surface representation of the GSTM2-2 active site. Surface color code is the same as in Fig. 4*A*, the GSH/NBDHEX σ-complex (*sticks with magenta carbons*). The H-site in this case seems larger, with a deeper cavity towards the core of the protein that is occupied by the NBDHEX nitro group. *C,* overlay of the GSTP1-1 and GSTM2-2 structures. GSTP1-1 residues (*sticks with green carbons*), GSTM2-2 residues with magenta carbons. The NBDHEX molecule occupies different positions in the two active sites. This is the result of the presence, in the GSTP1-1 H-site, of Ile^{104} and Arg^{13}, which gate the site and are topologically replaced by Ala^{111} and Leu^{12} in the GSTM2-2 active site, respectively.

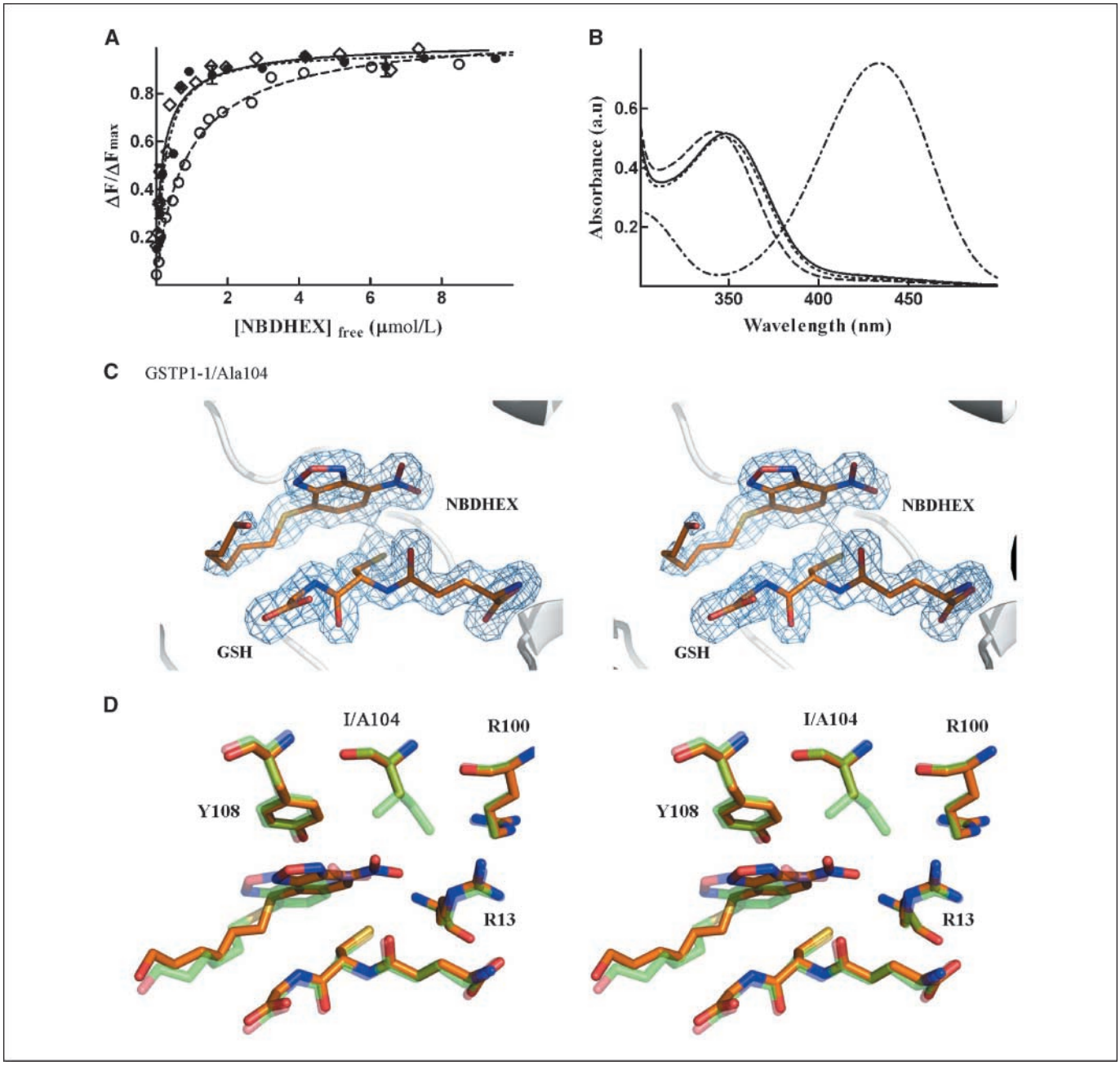

Figure 4. Analysis of the reaction of NBDHEX with GSTP1-1/Ile^{104}, GSTP1-1/Val^{104}, and GSTP1-1/Ala^{104}. *A,* the binding of NBDHEX was studied at 25°C and in the presence of 1 mmol/L of GSH, by following the quenching of the intrinsic fluorescence of the protein. Binding of NBDHEX to GSTP1-1/Val^{104} (—◇—), GSTP1-1/Ala^{104} (· · ·●· · ·), and GSTP1-1/Ile^{104} (- - -○- - -). *Points,* mean; *bars*, SD (n = 4); *lines,* the best fit of experimental data to Eq. A**.** *B,* the UV-visible spectrum of NBDHEX (50 μmol/L) in 0.1 mol/L of potassium phosphate buffer (pH 6.5), containing 1 mmol/L of GSH was recorded at 25°C before (- · -) and after the addition of two equivalents of either GSTP1-1/Ile^{104} (—), GSTP1-1/Val^{104} (· · ·), or GSTP1-1/Ala^{104} (- - -). The σ-complex absorption band formed by GSTP1-1/Ala^{104} was centered at 344 nm, whereas that formed by either GSTP1-1/Val^{104} or Ile^{104} (wild-type) variants showed a peak at 350 nm (a representative experiment out of three performed with similar results). *C,* crystal structure of the GSTP1-1/Ala^{104} variant in complex with GSH and NBDHEX. Stereoview of the protein active site. The σ_A-weighted 2Fo-Fc map, contoured at 1.0 σ (*blue mesh*), and GSH and NBDHEX (*sticks*). *D,* overlay of the structures of GSTP1-1 (*green carbons*) and of GSTP1-1/Ala^{104} variant (*orange carbons*). The NBDHEX molecule in the GSTP1-1/Ala^{104} structure is shifted by ~2 Å with respect to the wild-type structure and establishes a direct H-bond interaction with Arg^{13}.

with GSTM2-2, which is the human GST isozyme that displays the higher affinity for the compound (20).

In the case of GSTM2-2, we observe the presence of a σ-complex and thus provide a structural clue to the hypothesized mechanism of inhibition (see Fig. 1*A*; ref. 20). On the other hand, with GSTP1-1, we see a preconjugation state in which the NBDHEX molecule is bound to the enzyme but not conjugated. The reason for this difference might be due to the lack of diffusion-controlled motion of the active site region caused by the crystalline environment. However, we propose that in the GSTP1-1 structure, the σ-complex would occupy the same position of the unbound NBDHEX. This is suggested both by the shape of the H-site and by observing that a simple rotation of the GSH sulfur would be consistent with its addition to the benzoxadiazole ring C4 (see Fig. 1*B*).

A comparative analysis of GSTP1-1 and GSTM2-2 structures indicates that NBDHEX binds the two enzymes in a similar orientation and is stabilized through stacking interactions with aromatic side chains (Tyr^{108} for GSTP1-1 and Tyr^{115} for GSTM2-2). Aromatic stacking interactions with residues in the H-site are also the main contributors to the stabilization of drugs like ethacrynic acid and chlorambucil (40–42). However, unlike what happens with ethacrynic acid and chlorambucil binding to GSTP1-1, in which their polar groups point out of the H-site, in the case of NBDHEX, the benzoxadiazole nitro group constitutes the main driving force to dictate and stabilize binding to both GSTP1-1 and GSTM2-2, and is likely responsible for the higher affinity towards this compound (20, 41, 43). In the case of GSTM2-2, NBDHEX interacts directly with two positively charged arginines located at the bottom of the H-site. These residues provide stabilization when the σ-complex is formed and the nitro group acquires a net negative charge (see Fig. 2*B*). Conversely, in the GSTP1-1 structure, Arg^{13} only provides stabilization but indirectly via a water-mediated contact (see Fig. 1*C*). Of the two GSTM2-2 arginines, only one is topologically conserved in GSTP1-1 (Arg^{100}) but it is too distant from NBDHEX to help stabilize the molecule (see Fig. 3*C*). This is a consequence of the fact that Ile^{104}, a residue that is topologically replaced by an alanine in GSTM2-2, is located between the NBDHEX nitro group and Arg^{100}, and impedes further NBDHEX movement towards this positively charged residue. If this does not prevent the σ-complex from forming, as it is monitored by absorption spectra in solution, it certainly plays a role in diminishing the affinity of the compound for GSTP1-1 (see Fig. 3*C*). These considerations are confirmed by our mutagenesis data on residue Ile^{104}. We show here that replacement of the bulky isoleucine with valine (natural allelic variant) or alanine (the residue that replaces Ile^{104} in GSTM2-2) increases the affinity of GSTP1-1 for NBDHEX by 4-fold. This result may be clinically relevant because it implies that NBDHEX would be equally effective or better against those tumors in which the allelic variant GSTP1-1/Val^{104} is expressed. Moreover, when Ile^{104} is replaced by an alanine, not only does NBDHEX affinity for GSTP1-1 increase, but a blue-shift in the maximum absorption of the σ-complex spectrum is also observed, suggesting that in this mutant, NBDHEX finds a way to move further toward the positive charges and get higher stabilization. We confirmed this hypothesis by determining the structure of the GSTP1-1/Ala^{104} variant in complex with NBDHEX, which showed that the compound is shifted by ~2 Å towards Arg^{13}, displacing the water molecule and establishing a direct H-bond interaction between the benzoxadiazole ring nitro group and the Arg^{13} guanidine group (see Fig. 4*D*).

Can we infer from these data how to modify NBDHEX to inhibit GSTP1-1 with higher affinity? A possible route would be that of synthesizing molecules that retain the benzoxadiazole ring, to take advantage of the aromatic stacking interaction with Tyr^{108} and of the intrinsic stability of its σ-complex within the H-site. At the same time, a newly synthesized inhibitor should interact directly or more strongly with the positively charged Arg^{13}. This might be achieved by substituting the nitro group with other functional groups. Furthermore, because we showed that the NBDHEX hexanol moiety is only weakly involved in protein binding, a concurrent strategy might be that of modifying this part of the molecule with a different leaving group that has the potential to interact strongly with H-site residues. Future work in our laboratories will be aimed at testing several hypotheses suggested by the structural framework provided here.

Disclosure of Potential Conflicts of Interest

No potential conflicts of interest were disclosed.

Acknowledgments

Received 4/8/09; revised 7/24/09; accepted 8/10/09; published OnlineFirst 10/6/09.

Grant support: BeSSYII-ELISA grant agreement no. 226716, the Italian Ministero dell'Università e della Ricerca (MIUR), Alleanza Contro il Cancro-ISS, and MIUR, FIRB RBLA03B3KC_004 (A. Di Matteo).

The costs of publication of this article were defrayed in part by the payment of page charges. This article must therefore be hereby marked *advertisement* in accordance with 18 U.S.C. Section 1734 solely to indicate this fact.

We thank the beamline scientists at the European Synchrotron Research Facility (Grenoble, France) and at the "Helmholtz Zentrum Berlin fur Materialen und Energie-BeSSYII" (Berlin, Germany) for beamtime allocation and support.

References

1. Meijerman I, Beijnen JH, Schellens JH. Combined action and regulation of phase II enzymes and multidrug resistance proteins in multidrug resistance in cancer. Cancer Treat Rev 2008;34:505–20.
2. Townsend DM, Tew KD. The role of glutathione-S-transferase in anti-cancer drug resistance. Oncogene 2003;22:7369–75.
3. Hayes JD, Flanagan JU, Jowsey IR. Glutathione transferases. Annu Rev Pharmacol Toxicol 2005;45:51–88.
4. Oakley AJ. Glutathione transferases: new functions. Curr Opin Struct Biol 2005;15:716–23.
5. Sheehan D, Meade G, Foley VM, Dowd CA. Structure, function and evolution of glutathione transferases: implications for classification of non-mammalian members of an ancient enzyme superfamily. Biochem J 2001; 360:1–16.
6. Inoue T, Ishida T, Sugio K, Maehara Y, Sugimachi K. Glutathione S transferase Pi is a powerful indicator in chemotherapy of human lung squamous-cell carcinoma. Respiration 1995;62:223–27.
7. Ruiz-Gomez MJ, Souviron A, Martinez-Morillo M, Gil L. P-glycoprotein, glutathione and glutathione S-transferase increase in a colon carcinoma cell line by colchicine. J Physiol Biochem 2000;56:307–12.
8. Okuyama T, Maehara Y, Endo K, et al. Expression of glutathione S-transferase-pi and sensitivity of human gastric cancer cells to cisplatin. Cancer 1994;74:1230–36.
9. Grignon DJ, Abdel-Malak M, Mertens WC, Sakr WA, Shepherd RR. Glutathione S-transferase expression in renal cell carcinoma: a new marker of differentiation. Mod Pathol 1994;7:186–9.
10. Green JA, Robertson LJ, Clark A H. Glutathione S-transferase expression in benign and malignant ovarian tumours. Br J Cancer 1993;68:235–9.
11. Zhang L, Xiao Y, Priddy R. Increase in placental glutathione S-transferase in human oral epithelial dysplastic lesions and squamous cell carcinomas. J Oral Pathol Med 1994;23:75–9.
12. Katagiri A, Tomita Y, Nishiyama T, Kimura M, Sato S. Immunohistochemical detection of P-glycoprotein and GSTP1-1 in testis cancer. Br J Cancer 1993;68: 125–9.
13. Ban N, Takahashi Y, Takayama T, et al. Transfection of glutathione S-transferase (GST)-pi antisense complementary DNA increases the sensitivity of a colon cancer cell line to adriamycin, cisplatin, melphalan, and etoposide. Cancer Res 1996;56:3577–82.
14. Adler V, Yin Z, Fuchs SY, et al. Regulation of JNK signaling by GSTp. EMBO J 1999;18:1321–34.
15. Wang T, Arifoglu P, Ronai Z, Tew KD. Glutathione S-transferase P1-1 (GSTP1-1) inhibits c-Jun N-terminal kinase (JNK1) signaling through interaction with the C terminus. J Biol Chem 2001;276:20999–21003.
16. Adler V, Pincus MR. Effector peptides from glutathione-S-transferase-pi affect the activation of jun by jun-N-terminal kinase. Ann Clin Lab Sci 2004;34:35–46.
17. Asakura T, Sasagawa A, Takeuchi H, et al. Conformational change in the active center region of GST P1-1, due to binding of a synthetic conjugate of DXR with GSH, enhanced JNK-mediated apoptosis. Apoptosis 2007;12:1269–80.
18. Mahajan S, Atkins WM. The chemistry and biology of inhibitors and pro-drugs targeted to glutathione S-transferases. Cell Mol Life Sci 2005;62:1221–33.
19. Tew KD. Redox in redux: emergent roles for glutathione S-transferase P (GSTP) in regulation of cell signaling and S-glutathionylation. Biochem Pharmacol 2007;73:1257–69.
20. Ricci G, De Maria F, Antonini G, et al. 7-Nitro-2,1,3-benzoxadiazole derivatives, a new class of suicide inhibitors for glutathione S-transferases. Mechanism of action of potential anticancer drugs. J Biol Chem 2005; 280:26397–405.
21. Turella P, Cerella C, Filomeni G, et al. Proapoptotic activity of new glutathione S-transferase inhibitors. Cancer Res 2005;65:3751–61.
22. Turella P, Filomeni G, Dupuis ML, et al. A strong glutathione S-transferase inhibitor overcomes the P-glycoprotein-mediated resistance in tumor cells. 6-(7-Nitro-2,1,3-benzoxadiazol-4-ylthio)hexanol (NBDHEX) triggers a caspase-dependent apoptosis in

MDR1-expressing leukemia cells. J Biol Chem 2006; 281:23725–32.
23. Ascione A, Cianfriglia M, Dupuis ML, et al. The glutathione S-transferase inhibitor 6-(7-nitro-2,1,3-benzoxadiazol-4-ylthio)hexanol overcomes the MDR1-P-glycoprotein and MRP1-mediated multidrug resistance in acute myeloid leukemia cells. Cancer Chemother Pharmacol 2009;64:419–24.
24. Filomeni G, Turella P, Dupuis ML, et al. 6-(7-Nitro-2,1,3-benzoxadiazol-4-ylthio)hexanol, a specific glutathione S-transferase inhibitor, overcomes the multidrug resistance (MDR)-associated protein 1-mediated MDR in small cell lung cancer. Mol Cancer Ther 2008;7: 371–9.
25. Pasello M, Michelacci F, Scionti I, et al. Overcoming glutathione S-transferase P1-related cisplatin resistance in osteosarcoma. Cancer Res 2008;68:6661–8.
26. Lo HW, Ali-Osman F. Genetic polymorphism and function of glutathione S-transferases in tumor drug resistance. Curr Opin Pharmacol 2007;7:367–74.
27. Battistoni A, Mazzetti AP, Petruzzelli R, et al. Cytoplasmic and periplasmic production of human placental glutathione transferase in *Escherichia coli*. Protein Expr Purif 1995;6:579–87.
28. Lo Bello M, Battistoni A, Mazzetti AP, et al. Site-directed mutagenesis of human glutathione transferase P1-1. Spectral, kinetic and structural properties of Cys-47 and Lys-54 mutants. J Biol Chem 1995;270:1249–53.
29. Otwinowski Z, Minor W. Processing of X-ray diffraction data collected in oscillation mode. Methods Enzymol 1997;276:307–26.
30. Vagin A, Teplyakov A. An approach to multi-copy search in molecular replacement. Acta Crystallogr D Biol Crystallogr 2000;56:1622–4.
31. Raghunathan S, Chandross RJ, Kretsinger RH, Allison TJ, Penington CJ, Rule GS. Crystal structure of human class mu glutathione transferase GSTM2-2. Effects of lattice packing on conformational heterogeneity. J Mol Biol 1994;238:815–32.
32. Murshudov GN, Vagin A, Dodson EJ. Refinement of macromolecular structures by the maximum-likelihood method. Acta Crystallogr D Biol Crystallogr 1997;53:240–55.
33. Emsley P, Cowtan K. COOT: model-building tools for molecular graphics. Acta Crystallogr D Biol Crystallogr 2004;60:2126–32.
34. Oakley AJ, Lo Bello M, Battistoni A, et al. The structures of human glutathione transferase P1-1 in complex with glutathione and various inhibitors at high resolution. J Mol Biol 1997;274:84–100.
35. Laskowsky RA, MacArthur MW, Moss DS, Thornton JR. PROCHECK: a program to check the stereochemical quality of protein structures. J Appl Crystallogr 1993;26: 283–91.
36. Habig WH, Jakoby WB. Assays for differentiation of glutathione S-transferases. Methods Enzymol 1981;77: 398–405.
37. Ricci G, Caccuri AM, Lo Bello M, et al. Structural flexibility modulates the activity of human glutathione transferase P1-1. Role of helix 2 flexibility in the catalytic mechanism. J Biol Chem 1996;271:16187–92.
38. Caccuri AM, Ascenzi P, Antonini G, et al. Structural flexibility modulates the activity of human glutathione transferase P1-1. Influence of a poor co-substrate on dynamics and kinetics of human glutathione transferase. J Biol Chem 1996;271:16193–8.
39. Johansson A-S, Stenberg G, Widersten M, Mannervik B. Structure-activity relationships and thermal stability of human glutathione transferase P1-1 governed by the H-site residue 105. J Mol Biol 1998;278:687–98.
40. Oakley AJ, Rossjohn J, Lo Bello M, Caccuri AM, Federici G, Parker MW. The three-dimensional structure of the human Pi class glutathione transferase P1-1 in complex with the inhibitor ethacrynic acid and its glutathione conjugate. Biochemistry 1997;36:576–585.
41. Parker LJ, Ciccone S, Italiano LC, et al. The anti-cancer drug chlorambucil as a substrate for the human polymorphic enzyme glutathione transferase P1-1: kinetic properties and crystallographic characterisation of allelic variants. J Mol Biol 2008;380:131–44.
42. Awasthi S, Srivastava SK, Ahmad F, Ahmad H, Ansari GAS. Interactions of glutathione S-transferase-rr with ethacrynic acid and its glutathione conjugate. Biochim Biophys Acta 1993;1164:173–8.
43. Horton JK, Roy G, Piper JT, et al. Characterization of a chlorambucil-resistant human ovarian carcinoma cell line overexpressing glutathione S-transferase mu. Biochem Pharmacol 1999;58:693–702.